Available online at www.sciencedirect.com

ScienceDirect

Advances in Space Research 65 (2020) 2773–2781

ADVANCES IN SPACE RESEARCH (a COSPAR publication)

www.elsevier.com/locate/asr

Validation of International Reference Ionosphere model (IRI-2016) for F-region peak electron density height (hmF2): Comparison with Incoherent Scatter Radar (ISR) and ionosonde measurements at Millstone Hill

C.K. Mengist [a,b,*], S. Yadav [c,d], K. Kotulak [e], A. Bahar [f], S.-R. Zhang [g], K.-H. Seo [a,h,*]

[a] Research Center for Climate Sciences, Pusan National University, Busan, Republic of Korea
[b] Department of Physics, Adama Science and Technology University, Adama, Ethiopia
[c] Space Physics Laboratory, Vikram Sarabhai Space Centre, Trivandrum, India
[d] Institute for Space-Earth Environment Research, Nagoya University, Nagoya, Japan
[e] Space Radio-Diagnostics Research Centre, University of Warmia and Mazury, Olsztyn, Poland
[f] Indonesian National Institute of Aeronautics and Space, Jakarta, Indonesia
[g] Haystack Observatory, Massachusetts Institute of Technology, Westford, MA, USA
[h] Department of Atmospheric Sciences, Pusan National University, Busan, Republic of Korea

Received 8 November 2019; received in revised form 12 March 2020; accepted 13 March 2020
Available online 24 March 2020

Abstract

In this report, we have evaluated the performance of International Reference Ionosphere (IRI-2016) model in predicting the diurnal variation of F-region peak electron density height (hmF2) at Millstone Hill (MH, 42.6°N, 288.5°E) during the solar cycle 24 for both high and low-solar activity years. The new methodology is adopted to derive hmF2 values from the Incoherent Scatter Radar (ISR) measurements. The hmF2 derived from ISR along with ionosonde measurements operating at MH has been used to evaluate the performance of IRI-2016 model. The IRI-2016 model has three options to predict hmF2, namely, BSE-1979, AMTB-2013, and SHU-2015. The observed hmF2 from ISR and ionosonde are compared with all the three options provided by IRI-2016 to predict hmF2. Results show that hmF2 from IRI-2016, ISR and ionosonde exhibit similar diurnal variation. The deviations between measurements and model predictions were found to increase during nighttime. The SHU-2015 model emerged out to be the best in predicting the hmF2 values over MH as compared to other two options. The BSE-1979 option also provides reasonably better prediction as compared to the relatively latest AMTB-2013 options. Based on this statistical analyses, we recommend SHU-2015 option of IRI-2016 hmF2 model over MH area.

Keywords: IRI-2016; ISR; Ionosonde; hmF2

1. Introduction

There are numerous parameters that are typically used to characterize the state of the ionosphere. Some of these parameters are: NmF2, the maximum density of electrons in the F2 layer; hmF2, the height of the maximum electron density; and foF2, the maximum plasma frequency in the

* Corresponding authors at: Research Center for Climate Sciences, Pusan National University, Busan, Republic of Korea (C.K. Mengist). Department of Atmospheric Sciences, Pusan National University, Busan, Republic of Korea (K.-H. Seo).
E-mail addresses: chalachewkindie@yahoo.com (C.K. Mengist), khseo@pusan.ac.kr (K.-H. Seo).

https://doi.org/10.1016/j.asr.2020.03.017
0273-1177/

F2 layer. These parameters are important for terrestrial and satellite telecommunications so that they have been constantly monitored (Bremer et al., 2004; Bencze, 2005). Studies show that neutral meridional wind is derived from hmF2 data (Miller et al. 1986; Dyson et al., 1997; Liu et al., 2003). It is important to evaluate the performance of International Reference Ionosphere (IRI) to predict hmF2 because, among many applications, IRI-hmF2 can be used to produce the global scale midlatitude meridional wind climatology (Miller et al., 1997).

The IRI is a standard model of the terrestrial ionosphere and recognized in an International Organization for Standardization (ISO). The IRI is a joint project supported by the Committee on Space Research (COSPAR) and the International Union of Radio Science (URSI) with the goal of developing and improving an international standard for the parameters in Earth's ionosphere (Bilitza et al., 2014, 2017). IRI working group has given high priority to improve the model with new data source available and new technique. The prediction of IRI hmF2 are evaluated with ionosonde data at different locations for different seasons and solar activity levels (Zhang et al., 2004; Yadav et al., 2010; Magdaleno et al., 2011; Kalita et al., 2015; Tsagouri et al., 2018 and reference therein). Magdaleno et al. (2011) reported that IRI hmF2 and ionosonde hmF2 show disagreement and proposed an empirical model to improve IRI model performance during geomagnetically quiet conditions over the ionosonde locations used in their study. The validation of IRI hmF2 at equator latitude during low solar activity (Lee et al., 2008; Ehinlafa et al., 2010; Shreedevi et al., 2018), at low and middle latitudes during low solar activity (Sethi et al., 2008; Yadav et al., 2010, 2013), and at high latitudes during high solar activity (Oyeyemi et al., 2010; Shreedevi et al., 2019) shows deviation from ionosonde measurements.

The IRI-2016 model has three options to predict F2 peak hmF2: BSE-1979, AMTB-2013, and SHU-2015 (Bilitza et al., 2017). BSE-1979 model is derived based on monthly median M3000F2 values obtained by using ~150 ionosondes around the globe (Bilitza et al., 1979). AMTB-2013 model is developed based on 26 digisonde data from the Global Ionosphere Radio Observatory (GIRO) network during the period 1998–2006 (Altadill et al., 2013). SHU-2015 is based on radio occultation data from COSMIC (years: 2006–2012; ~3,500,000), GRACE (2007–2011; ~100,000), CHAMP (2001–2008; ~300,000), and hmF2 data from 62 digisondes during 1987–2012 (Shubin, 2015). The detailed information about these three options can be found in Bilitza et al. (2017). It is required to provide the IRI user community the ability to compare different hmF2 model predictions against various data sources which would eventually help to improve the accuracy of these models and measurement techniques.

In this report, the performance of IRI-2016 predicted hmF2 is evaluated during the solar cycle 24 (2009–2016). The three options of IRI-2016 hmF2 (BSE-1979, AMTB-2013, and SHU-2015) are compared with experimentally observed Millstone Hill (MH) Incoherent Scatter Radar (ISR) hmF2 data and ionosonde hmF2 data during 2009–2016. This paper is organized as follows: Section 2 presented data and methodology used, and Section 3 discusses IRI-2016 model performance during the solar cycle 24. We also present a new technique to derive hmF2 from the irregularly spaced measurement data points on the vertical profile of electron density. Comparison between observed hmF2 and IRI hmF2 for all the three options is performed by evaluating the root-mean-squared-error (RMSE). Finally, Section 4 gives conclusion.

2. Data and methodology

The primary data source for the present study is ISR and ionosonde operating at Millstone Hill (geographic 42.6°N, 288.5°E). The solar local time (LT) lags behind the universal time by approximately 5 h i.e., LT ≈ UT − 5. The ISR data are obtained from Madrigal Database (http://openmadrigal.org/). The MH ISR system operates with a zenith-directed 68 m fixed parabolic antenna and details of MH ISR data is available at Holt et al. (2002). Millstone Hill ionosonde data are available at GIRO DIDbase (http://giro.uml.edu/didbase/scaled.php). Ionosonde data from GIRO DIDbase are obtained using the Automatic Real-Time Ionogram Scaler with True height (ARTIST) software (Reinisch and Galkin, 2011).

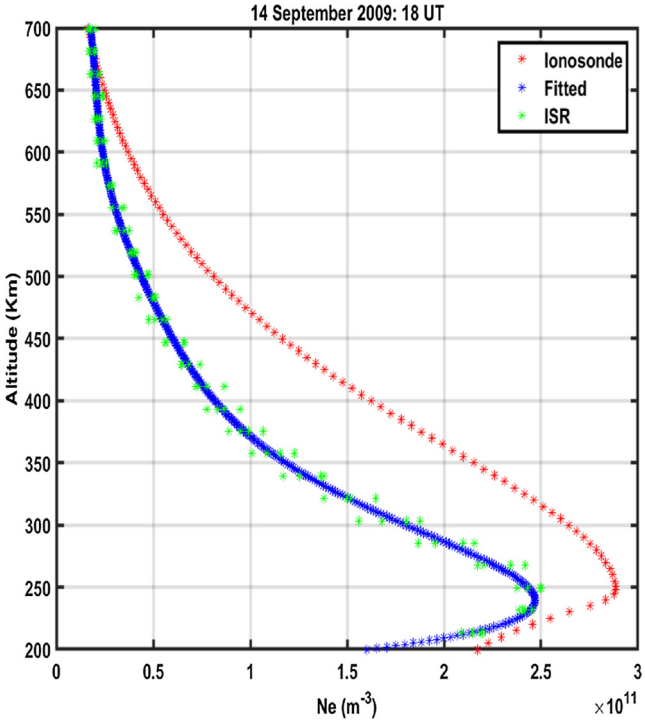

Fig. 1. Electron density profile on 14 September 2009. Green scatter represent the ISR derived electron density profile and blue curve depict the fitted curve. Red curve shows electron density profile from MH ionosonde observation. (For interpretation of the references to color in this figure legend, the reader is referred to the web version of this article.)

Ionosonde observations provide ionospheric electron density profile including F2 layer peak, and hmF2 is obtained from the true height inversion program NHPC (Huang and Reinisch, 1996). The electron density profile derived from ISR and ionosonde measurements has been used during the solar cycle 24 (2009–2016) to derive hmF2. All the available geomagnetic quiet days during 2009–2016 have been used for the study. The Fortran source code of IRI-2016 is available at http://irimodel.org. In this study CCIR option is used to generate IRI hmF2. CCIR option is recommended over continent areas (Ssessanga et al., 2015).

The method adapted for deriving hmF2 values from the ISR electron density profile is described as follows. First of all, the irregularly spaced vertical electron density profiles from MH ISR are collected in 1-hour window and fitted with a polynomial function as follows:

Given M points, there is a unique polynomial

$$p(x) = \sum_{i=1}^{M} c_i x^{i-1} \tag{1}$$

satisfying M equations

$$f(b_j) = \sum_{i=1}^{M} c_i b_j^{i-1} \tag{2}$$

where j = 1, 2, 3, …, M.

Let $\boldsymbol{f} = [f(b_1) \cdots f(b_M)]^T$ is a vector of the function values and $\boldsymbol{c} = [c_1 \cdots c_M]^T$ is a vector of the polynomial coefficient.

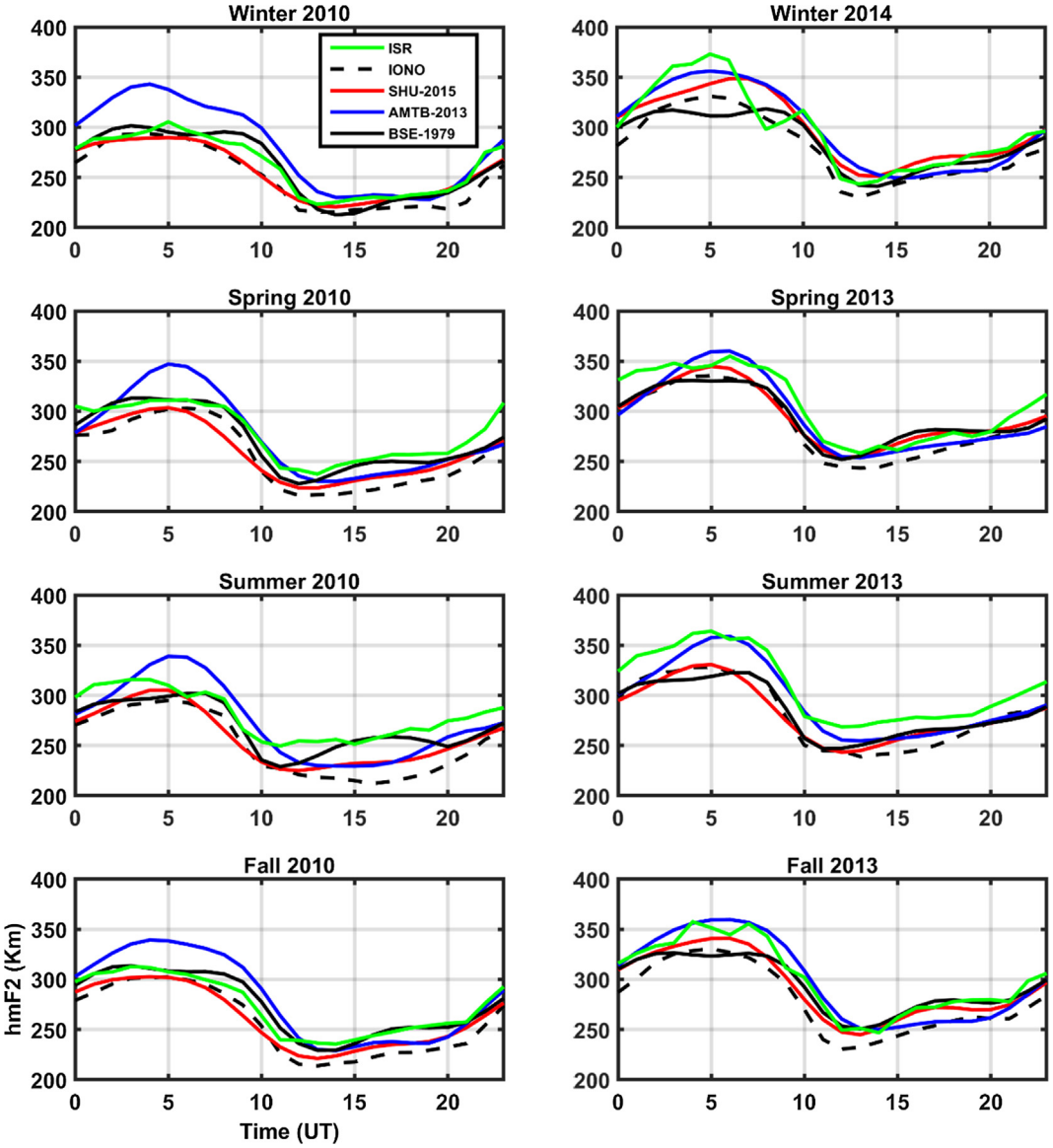

Fig. 2. Diurnal variation of ISR hmF2 (green), ionosonde hmF2 (black dashed line), SHU-2015 hmF2 (red), AMTB-2013 hmF2 (blue), and BSE-1979 hmF2 (black solid line) during solar minimum (2010) and solar maximum (2013 and 2014). (For interpretation of the references to color in this figure legend, the reader is referred to the web version of this article.)

Eq. (2) can be written using the Vandermonde matrix, V, as

$$\boldsymbol{f} = V(b_1, \cdots, b_M).\boldsymbol{c} \tag{3}$$

The polynomial coefficient vector **c** is computed as

$$\boldsymbol{c} = V(b_1, \cdots, b_M)^{-1}.\boldsymbol{f} \tag{4}$$

After fitting the electron density profile, the height of the peak electron density (hmF2) has been found out. Fig. 1 depicts the ISR (green) and ionosonde (red) derived vertical electron density profile on 14 September 2009 at 1800 UT. The blue in the figure shows the polynomial fitting over the data as described above. The ISR and ionosonde electron density profile shows a peak at around ~240 km and ~250 km, respectively and decreased exponentially thereafter. Owing to irregularly spaced vertical electron density profiles in the ISR observations, it is difficult to decipher the peak electron density height. However, by using the fitted curve, the height of peak electron density (hmF2) can be found out.

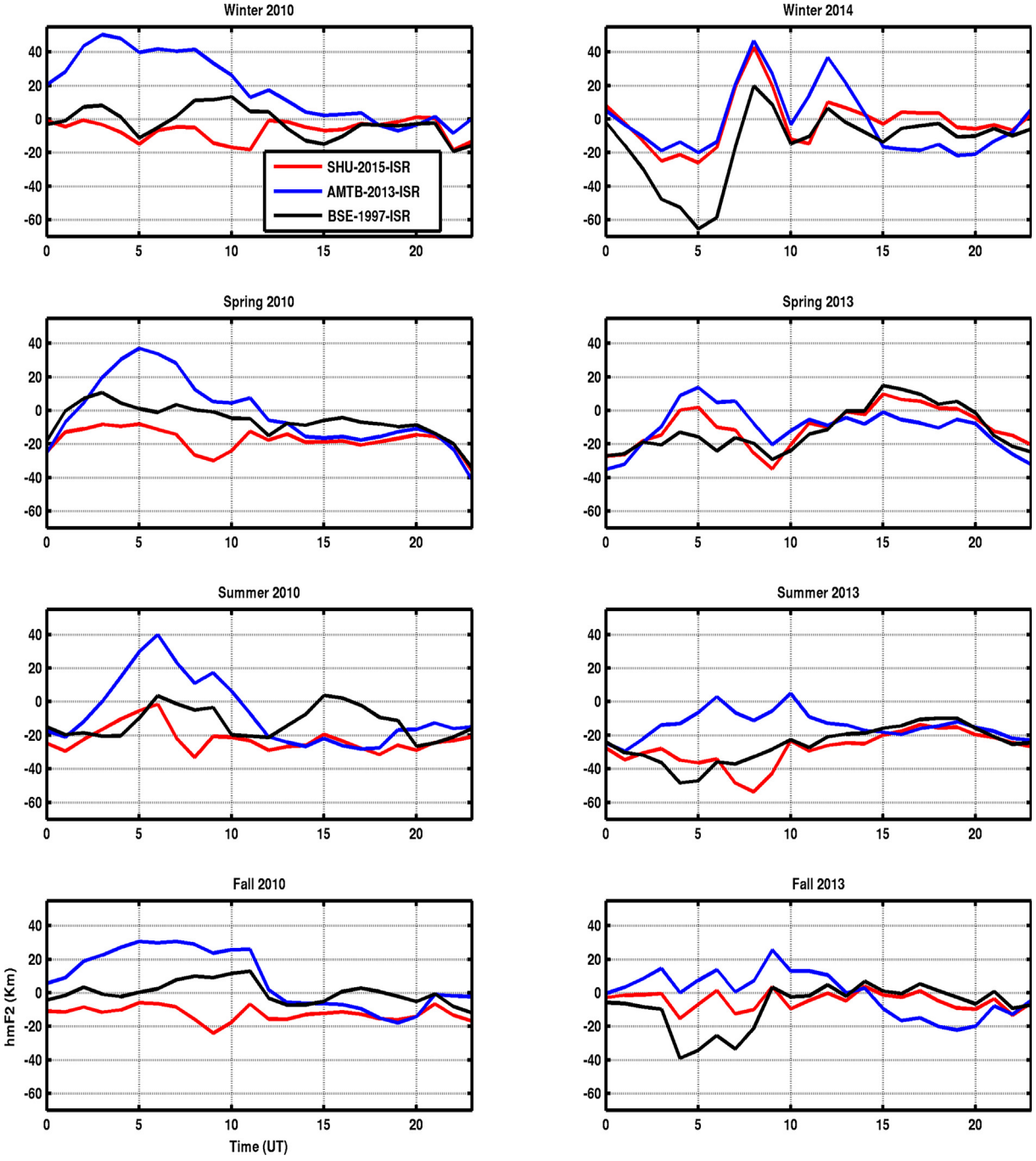

Fig. 3. Diurnal variation of difference between IRI hmF2 and ISR hmF2 during solar minimum (2010) and solar maximum (2013 and 2014). SHU-2015 hmF2, AMTB-2013 hmF2, and BSE-1979 hmF2 are given in red, blue, and black. (For interpretation of the references to color in this figure legend, the reader is referred to the web version of this article.)

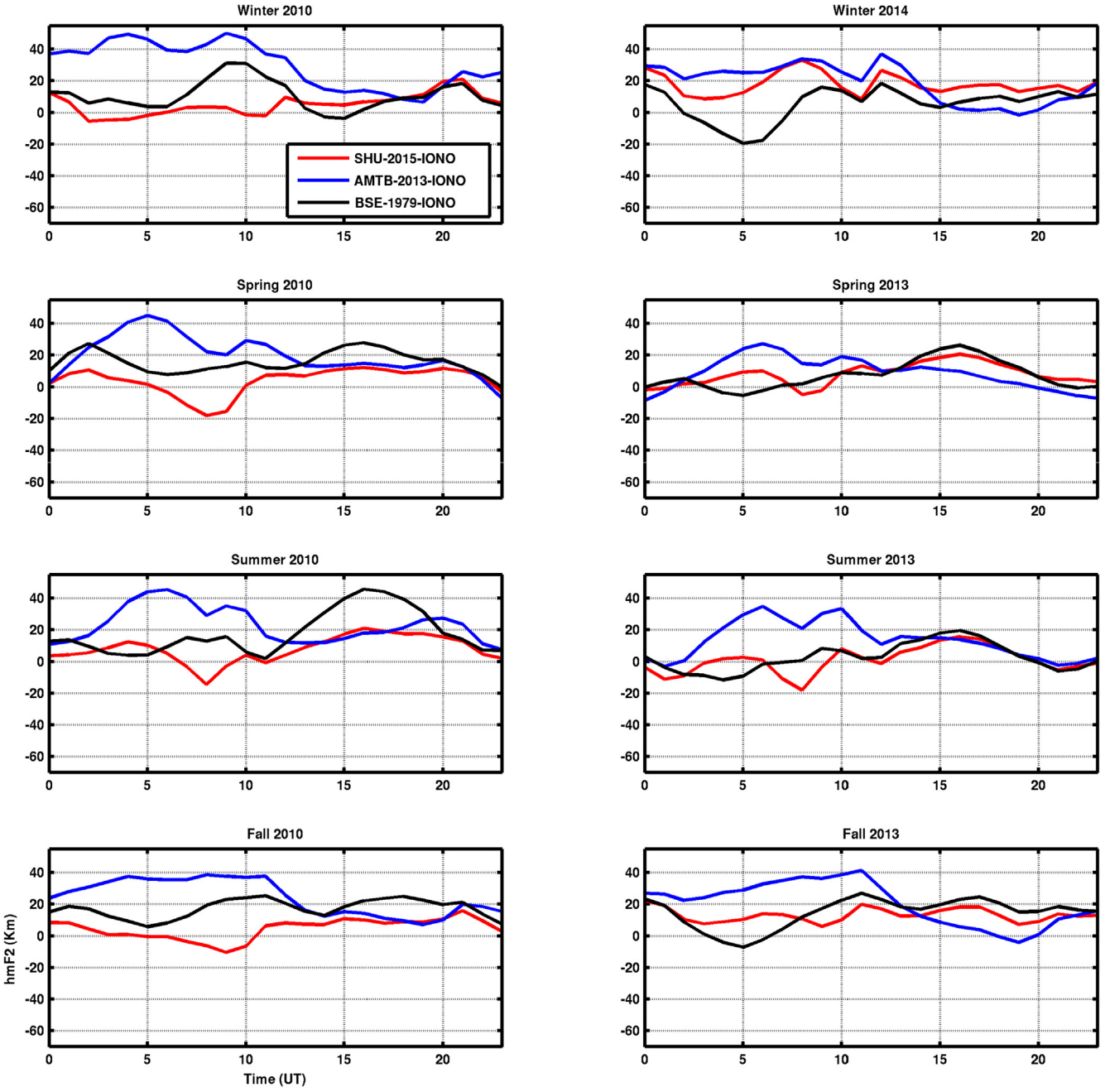

Fig. 4. Same as Fig. 3 but difference between IRI hmF2 and ionosonde hmF2.

Table 1
RMSE from the comparison between IRI hmF2 predictions with ISR hmF2 and ionosonde hmF2 during high-solar activity and low-solar activity.

	Season	SHU-2015		AMTB-2013		BSE-1979	
		ISR	IONO	ISR	IONO	ISR	IONO
Solar Minimum	Winter	11.70	20.40	25.67	39.15	12.48	23.39
	Spring	27.51	19.08	27.36	28.96	23.72	24.11
	Summer	29.91	18.00	27.08	29.91	21.77	24.83
	Fall	17.93	14.77	20.98	29.48	13.28	22.39
Solar Maximum	Winter	12.56	25.56	20.05	28.47	16.77	20.54
	Spring	24.72	19.27	27.66	20.46	27.64	20.03
	Summer	30.57	18.37	22.71	23.73	29.47	18.82
	Fall	12.45	19.83	17.98	27.98	16.32	22.56

The performance of IRI-2016 hmF2 model has been evaluated by calculating the root-mean-squared-error (RMSE) between the predicted and observed hmF2 values from ISR and ionosonde. The RMSE of the IRI-2016 hmF2 model prediction with respect to MH ISR and ionosonde is defined as

$$RMSE = \sqrt{\frac{\sum_{i=1}^{n} (X_{obs,i} - X_{model,i})^2}{n}} \quad (5)$$

where n is the number of data points, X_{obs} is observed hmF2 from MH ISR and ionosonde, X_{model} is IRI-2016 model prediction of hmF2 using SHU-2015, AMTB-2013, and BSE-1979.

3. Results and discussions

Seasonal average values of the observed hmF2 is calculated from the daily hourly values to represent different seasonal values of hmF2. Fig. 2 shows the diurnal variation of observation hmF2 (MH ISR and ionosonde) and IRI hmF2 for winter, spring, summer, and fall during the year 2010 which represent low-solar and during the year 2013 and 2014 to represent high-solar activity. The figure depicted ISR hmF2 (green), ionosonde (black dashed), SHU-2015 hmF2 (red), AMTB-2013 hmF2 (blue), and BSE-1979 hmF2 (black solid). At mid-high latitude, during daytime the plasma moves downward along the Earth's magnetic field direction and during nighttime the plasma elevated up by the equatorward winds (Fuller-Rowell et al., 2008). This process produces diurnal variation of hmF2 as shown in the figure, with lower values of hmF2 during daytime and higher values of hmF2 during nighttime. Overall, IRI hmF2 predictions follow the hmF2 diurnal variation observed from ISR and ionosonde data; showing larger values during solar maximum than during solar minimum. ISR hmF2 observations show larger values during summer while lower values are observed during winter. The mean ISR hmF2 and ionosonde hmF2 during solar minimum winter is 263 Km and 250 km; during solar maximum winter is 298 Km and 280 Km, respectively. The mean values of hmF2 from ISR and ionosonde during solar minimum summer shows 280 Km and 250 Km; during solar maximum summer shows 309 Km and 282 Km, respectively. Figs. 3 and 4 show the difference between IRI hmF2 and ISR hmF2, IRI hmF2 and ionosonde hmF2, respectively, during solar minimum (2010) and solar maximum (2013 and 2014). During nighttime SHU-2015 hmF2 underestimates ISR hmF2. Similarly, AMTB-2013 hmF2 overestimates ISR hmF2 during nighttime. The three IRI hmF2 options overestimate ionosonde hmF2 during nighttime except BSE-1979 for solar maximum. All IRI hmF2 options underestimate ISR hmF2 and ionosonde hmF2 during daytime.

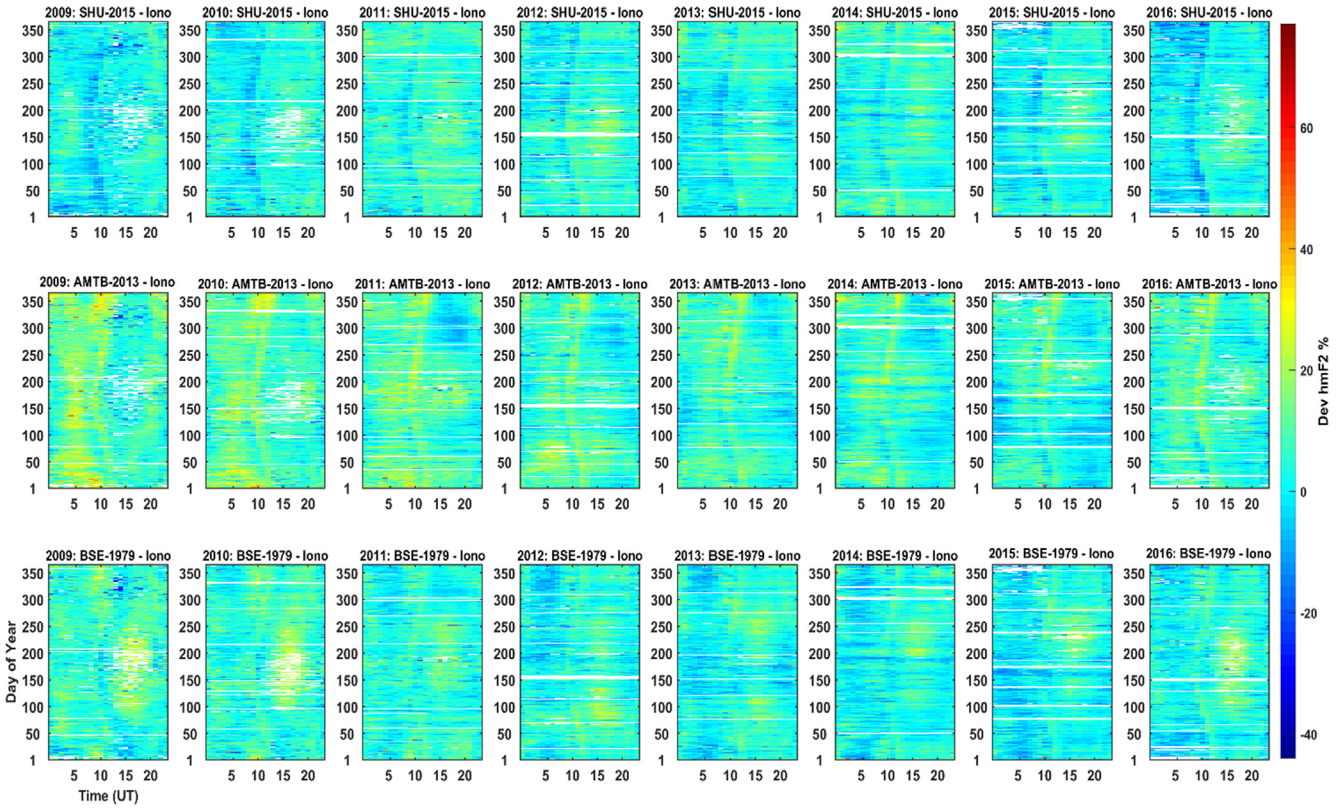

Fig. 5. Percentage deviation of IRI hmF2 model options relative to ionosonde observation during 2009 to 2016. The white color from the plot is means no data observed by ionosonde.

In order to evaluate qualitative performance of IRI, we have performed the statistical analysis to estimate the root mean square error (RMSE) between the observation and IRI predicted hmF2 for all the three options. The results of the analysis are depicted in Table 1. The least RMSE between the observations and model prediction is observed for SHU-2015 and BSE-1979. This fact is true for almost all the seasons and both solar activity levels. Seasonally, lowest values of RMSE occur during winter and highest values of RMSE occurs during the summer season. It is observed that generally the performance of IRI remains better under solar minimum conditions as compared to solar maximum (Pandey et al., 2003).

We also have examined the percentage deviation of the IRI predictions with respect to the ionosonde measured hmF2 over MH. The percentage deviation between IRI and ionosonde measurements is obtained as [(hmF2IRI-hmF2obs)/hmF2obs]. Fig. 5 depicts the percentage deviation of IRI hmF2 model options relative to ionosonde observation during 2009 to 2016. The white color from the plot means no data observed by ionosonde during that time. The diurnal variation of percentage deviation can be noted for all the solar activity levels. The IRI predictions appeared considerable better for SHU-2015 as compared to BSE-1979. Generally, the percentage deviation for SHU-2015 remained around ±20%, whereas for AMTB-2013 it increased to ±40%, and for BSE-1979 it remained around ±30%. From Figs. 3 and 4, the maximum deviation was observed during midnight to the morning sector where the IRI predicted values were seen to overestimate the measurements. This could be attributed to the fact that nighttime ionosphere is primarily driven by dynamical effect (Fuller-Rowell et al., 2008). The nighttime thermospheric wind are known to be equatorward which pushes the ionosphere up along the geomagnetic field lines, causing increase in hmF2.

Fig. 6 depicts the overview of the RMSE analysis applied between ISR measurements and IRI prediction

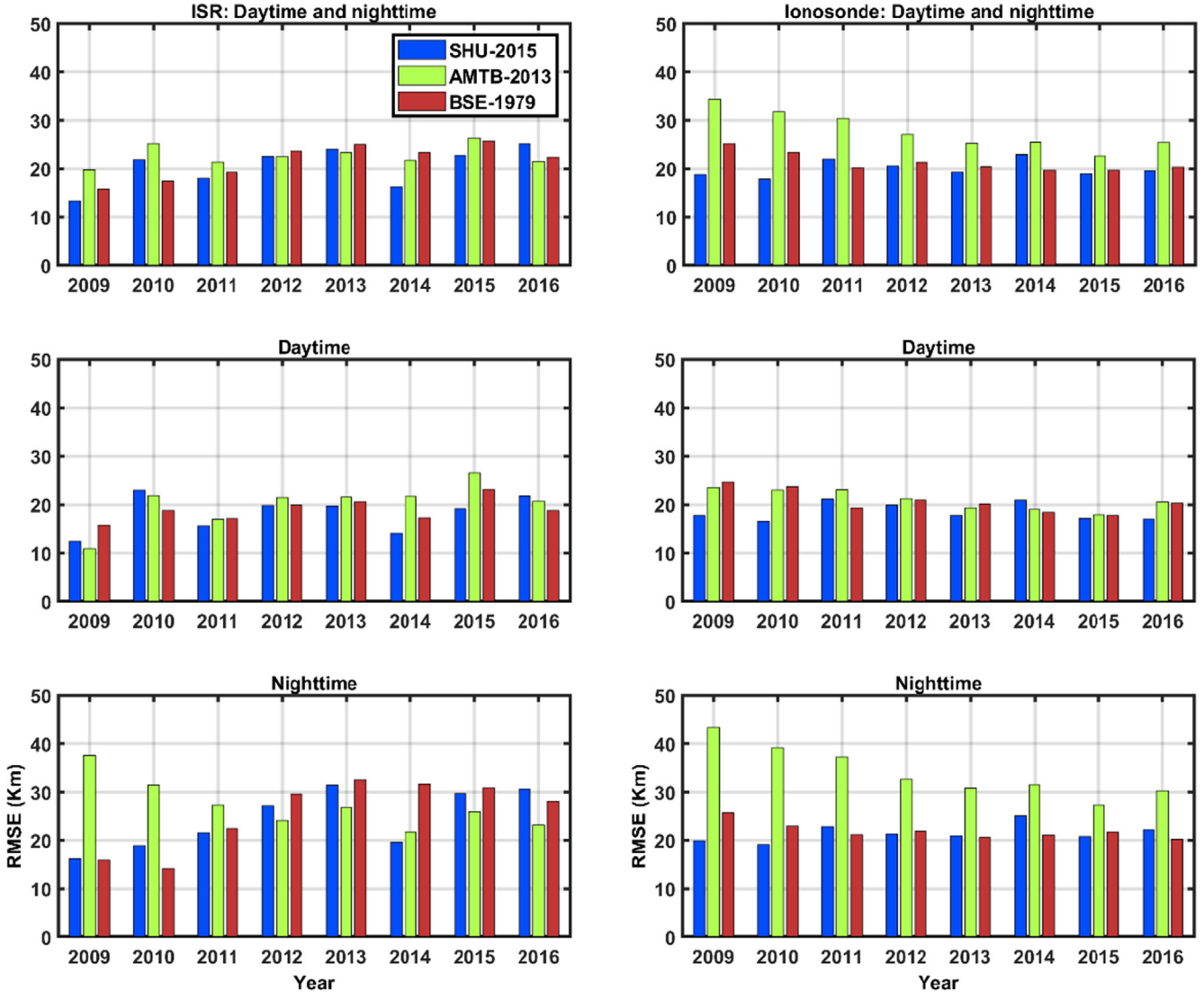

Fig. 6. RMSE of IRI hmF2 model relative to ISR(left) and ionosonde (right) observation during daytime and nighttime for different years.

(left) and ionosonde measurements and IRI prediction (right). The different panels of Fig. 6 depict the results for ISR and ionosonde measurements during the entire day, daytime and nighttime. The RMSE for different options of IRI is depicted by different colors. It can be seen that RMSE shows the lowest values for SHU-2015 for almost all years during all day when compared with the other options. RMSE was found to be as low as 13 Km compared with ISR and 18 Km compared with ionosonde. On the other hand, the RMSE for AMTB-2013 option appeared to exceed 30 Km and 40 Km during nighttime using ISR and ionosonde, respectively. The RMSE appeared to be least for daytime where it reached values of 11 Km while the maximum RMSE was observed during nighttime for all the options.

4. Summary and conclusions

We have evaluated the performance of IRI-2016 model for all the three hmF2 options (SHU-2015, AMTB-2013, and BSE-1979) during the solar cycle 24. The analysis revealed that the best option for the prediction of hmF2 at mid-latitude station like MH was SHU-2015. It is worth noting that BSE-1979 option also provides reasonably good predictions for hmF2 as compared to the relatively latest AMTB-2013 version. The daytime hmF2 values show reasonable agreement with the model predictions as compared to the nighttime values. The RMSE was found to be lower for the low solar activity as compared to high-solar activity levels. It is worth noting that RMSE using ISR data increased for the declining phase of the solar activity.

In addition to the evaluation of IRI, this work also provides a new methodology for estimating the hmF2 values using ISR measurements. The exponential fit was used to derive hmF2 from irregularly spaced vertical profile of electron density. Although we recommend SHU-2015 option for the prediction of hmF2 over MH, we suggest some more statistical analyses between observations and model predictions for different solar cycles and seasons.

Acknowledgments

The authors are acknowledging a COSPAR capacity building workshop IRI 2017 organizers, and National Central University (Taiwan). C. K. Mengist, S. Yadav, K. Kotulak, and A. Bahar are financially supported by a COSPAR capacity building IRI 2017 to attend the training and workshop. K.-H. Seo was supported by the National Research Foundation of Korea (NRF) grant funded by the Korea government (MSIP) (No. NRF-2020R1A2C2009414). We also would like to thank Professor Bilitza for providing this research topic. The Fortran source code of IRI-2016 is available at http://irimodel.org. The MH ISR data are available at http://openmadrigal.org/. Millstone Hill ionosonde data are from GIRO DIDbase (http://giro.uml.edu/didbase/scaled.php). The MH ISR observations and analysis at MIT Haystack Observatory are supported by cooperative agreement AGS- 1762141 between the US National Science Foundation and the Massachusetts Institute of Technology.

References

Altadill, D., Magdaleno, S., Torta, J.M., Blanch, E., 2013. Global empirical models of the density peak height and of the equivalent scale height for quiet conditions. Adv. Space Res. 52 (10), 1756–1769. https://doi.org/10.1016/j.asr.2012.11.018.

Bencze, P., 2005. On the long-term change of ionospheric parameters. J. Atmos. Sol. Terr. Phys. 67 (14), 1298–1306. https://doi.org/10.1016/j.jastp.2005.06.020.

Bilitza, D., Altadill, D., Truhlik, V., Shubin, V., Galkin, I., Reinisch, B., Huang, X., 2017. International Reference Ionosphere 2016: From ionospheric climate to real-time weather predictions. Space Weather 15 (2), 418–429. https://doi.org/10.1002/2016SW001593.

Bilitza, D., Altadill, D., Zhang, Y.L., Mertens, C., Truhlik, V., Richards, P., McKinnell, L.A., Reinisch, B., 2014. The International Reference Ionosphere 2012–a model of international collaboration. J. Space Weather Space Climate 4 (10), 689–721. https://doi.org/10.1051/swsc/2014004.

Bilitza, D., Sheikh, N.M., Eyfrig, R., 1979. A global model for the height of the F2-peak using M(3000)F2 values from the CCIR numerical map. Telecommun. J. 46, 549–553.

Bremer, J., Alfonsi, L.U., Bencze, P., Lastovicka, J., Mikhailov, A.V., Rogers, N., 2004. Long-term trends in the ionosphere and upper atmosphere parameters. Ann. Geophys. 47 (2–3 Sup.). https://doi.org/10.4401/ag-3283.

Dyson, P.L., Davies, T.P., Parkinson, M.L., Reeves, A.J., Richards, P.G., Fairchild, C.E., 1997. Thermospheric neutral winds at southern mid-latitudes: A comparison of optical and ionosonde hmF2 methods. J. Geophys. Res. 102 (A12), 27189–27196. https://doi.org/10.1029/97JA02138.

Ehinlafa, O.E., Falaiye, O.A., Adeniyi, J.O., 2010. Comparison of observed hmF2 and IRI 2007 model with M (3000) F2 estimation of hmF2 at low solar activity for an equatorial station. Adv. Space Res. 46 (1), 89–93. https://doi.org/10.1016/j.asr.2010.02.018.

Fuller-Rowell, T.J., Richmond, A.D., Maruyama, N., 2008. Global modeling of storm-time thermospheric dynamics and electrodynamics. Geophys Monogr. Series 181, 187–200.

Holt, J.M., Zhang, S., Buonsanto, M.J., 2002. Regional and local ionospheric models based on Millstone Hill incoherent scatter radar data. Geophys. Res. Lett. 29 (8), 1207. https://doi.org/10.1029/2002GL014678.

Huang, X., Reinisch, B.W., 1996. Vertical electron density profiles from the Digisonde network. Adv. Space Res. 18 (6), 121–129. https://doi.org/10.1016/j.asr.2016.12.008.

Kalita, B.R., Bhuyan, P.K., Yoshikawa, A., 2015. NmF2 and hmF2 measurements at 95° E and 127° E around the EIA northern crest during 2010–2014. Earth, Planets Sp. 67 (1), 186–207. https://doi.org/10.1186/s40623-015-0355-3.

Lee, C.C., Reinisch, B.W., Su, S.Y., Chen, W.S., 2008. Quiet-time variations of F2-layer parameters at Jicamarca and comparison with IRI-2001 during solar minimum. J. Atmos. Sol. Terr. Phys. 70 (1), 184–192. https://doi.org/10.1016/j.jastp.2007.10.008.

Liu, L., Luan, X., Wan, W., Lei, J., Ning, B., 2003. Seasonal behavior of equivalent winds over Wuhan derived from ionospheric data in 2000–2001. Adv. Space Res. 32 (9), 1765–1770. https://doi.org/10.1016/S0273-1177(03)90474-1.

Magdaleno, S., Altadill, D., Herraiz, M., Blanch, E., de La Morena, B., 2011. Ionospheric peak height behavior for low, middle and high latitudes: A potential empirical model for quiet conditions—Comparison with the IRI-2007 model. J. Atmos. Sol. Terr. Phys. 73 (13), 1810–1817. https://doi.org/10.1016/j.jastp.2011.04.019.

Miller, K.L., Lemon, M., Richards, P.G., 1997. A meridional wind climatology from a fast model for the derivation of meridional winds

from the height of the ionospheric F2 region. J. Atmos. Sol. Terr. Phys. 59 (14), 1805–1822. https://doi.org/10.1016/S1364-6826(97)00025-4.

Miller, K.L., Torr, D.G., Richards, P.G., 1986. Meridional winds in the thermosphere derived from measurement of F2 layer height. J. Geophys. Res. 91 (A4), 4531–4535. https://doi.org/10.1029/JA091iA04p04531.

Oyeyemi, E.O., Adewale, A.O., Adeloye, A.B., Akala, A.O., 2010. Comparison between IRI-2001 predictions and observed measurements of hmF2 over three high latitude stations during different solar activity periods. J. Atmos. Sol. Terr. Phys. 72 (9–10), 676–684. https://doi.org/10.1016/j.jastp.2010.03.009.

Pandey, V.K., Sethi, N.K., Mahajan, K.K., 2003. Dependence of F2-peak height on solar activity: a study with incoherent scatter measurements. Adv. Space Res. 31 (3), 543–548. https://doi.org/10.1016/S0273-1177(03)00049-8.

Reinisch, B.W., Galkin, I.A., 2011. Global ionospheric radio observatory (GIRO). Earth. Planets Sp. 63 (4), 377–381. https://doi.org/10.5047/eps.2011.03.001.

Ssessanga, N., Kim, Y.H., Kim, E., Kim, J., 2015. Regional optimization of the IRI-2012 output (TEC, foF2) by using derived GPS-TEC. J. Korean. Phys. Soc. 66 (10), 1599–1610. https://doi.org/10.3938/jkps.66.1599.

Sethi, N.K., Dabas, R.S., Sharma, K., 2008. Comparison between IRI predictions and digital ionosonde measurements of hmF2 at New Delhi during low and moderate solar activity. J. Atmos. Sol. Terr. Phys. 70 (5), 756–763. https://doi.org/10.1016/j.jastp.2007.10.009.

Shubin, V.N., 2015. Global median model of the F2-layer peak height based on ionospheric radio-occultation and ground-based Digisonde observations. Adv. Space Res. 56 (5), 916–928. https://doi.org/10.1016/j.asr.2015.05.029.

Shreedevi, P.R., Choudhary, R.K., Yu, Y., Thomas, E.G., 2019. Morphological study on the ionospheric variability at Bharati, a polar cusp station in the southern hemisphere. J. Atmos. Sol. Terr. Phys. 193. https://doi.org/10.1016/j.jastp.2019.105058.

Shreedevi, P.R., Choudhary, R.K., Yadav, S., Thampi, S., Ajesh, A., 2018. Variation of the TEC at a dip equatorial station, trivandrum and a mid latitude station, hanle during the descending phase of the solar cycle 24 (2014–2016). J. Atmos. Sol. Terr. Phys. 179, 425–434. https://doi.org/10.1016/j.jastp.2018.09.010.

Tsagouri, I., Goncharenko, L., Shim, J.S., Belehaki, A., Buresova, D., Kuznetsova, M.M., 2018. Assessment of current capabilities in modeling the ionospheric climatology for space weather applications: foF2 and hmF2. Space Weather 16, 1930–1945. https://doi.org/10.1029/2018SW002035.

Yadav, S., Dabas, R.S., Das, R.M., Upadhayaya, A.K., Gwal, A.K., 2013. Temporal and spatial variation of Equatorial ionization anomaly by using multistation ionosonde data for the 19th solar cycle over the Indian region. Adv. Space Res. 51, 1253–1265. https://doi.org/10.1016/j.asr.2012.11.009.

Yadav, S., Dabas, R.S., Das, R.M., Upadhayaya, A.K., Sharma, K., Gwal, A.K., 2010. Diurnal and seasonal variation of F2-layer ionospheric parameters at equatorial ionization anomaly crest region and their comparison with IRI-2001. Adv. Space Res. 45, 361–367. https://doi.org/10.1016/j.asr.2009.08.018.

Zhang, M.L., Shi, J.K., Wang, X., Radicella, S.M., 2004. Ionospheric variability at low latitude station: Hainan, China. Adv. Space Res. 34 (9), 1860–1868. https://doi.org/10.1016/j.asr.2004.04.005.